*Original Article*

Check for updates

Available online at
www.heca-analitika.com/ljes

**Leuser Journal of Environmental Studies**

Vol. 2, No. 1, 2024

# Characterization of Geochemical and Isotopic Profiles in the Southern Zone Geothermal Systems of Mount Seulawah Agam, Aceh Province, Indonesia

**Andi Lala [1,2], Muhammad Yusuf [2,3], Rivansyah Suhendra [4], Nur Balqis Maulydia [1], Dian Budi Dharma [1,5], Saiful Saiful [2] and Rinaldi Idroes [1,2,*]**

[1] Graduate School of Mathematics and Applied Sciences, Universitas Syiah Kuala, Banda Aceh 23111, Indonesia; andi_lala@usk.ac.id (A.L.); maulydiabalqis@gmail.com (N.B.M); dharmalampineung@yahoo.co.id (D.B.D); rinaldi.idroes@usk.ac.id (R.I.)
[2] Department of Chemistry, Faculty of Mathematics and Natural Sciences, Universitas Syiah Kuala, Banda Aceh 23111, Indonesia; iamyusufibrahim@gmail.com (M.Y.); saiful@usk.ac.id (S.S.)
[3] Department of Pharmacy, STIKES Assyifa Aceh, Aceh 23242, Indonesia
[4] Department of Information Technology, Faculty of Engineering, Universitas Teuku Umar, Aceh Barat 23681, Indonesia; rivansyahsuhendra@utu.ac.id (R.S.)
[5] Energy and Mineral Resources Agency of Aceh Province, Banda Aceh, Indonesia

***** Correspondence: rinaldi.idroes@usk.ac.id

**Article History**

Received 22 February 2024
Revised 5 April 2024
Accepted 18 April 2024
Available Online 29 April 2024

**Keywords**:
Cations
Anions
Isotopes
Mount Seulawah Agam
Geochemical
Geothermometer
Reservoir

**Abstract**

The Seulawah Agam geothermal area exhibits significant potential as a source of energy for power generation, with an estimated capacity of 130 MW. Geological and geochemical investigations indicate that the Seulawah Agam geothermal system is part of the extensive Sumatra Fault. Analysis of the geochemical composition of geothermal water at the South Zone manifestation location of Mount Seulawah Agam, Aceh Province-Indonesia, involves examining cation ($K^+$, $Na^+$, $Ca^{2+}$, and $Mg^{2+}$), anion ($Cl^-$, $HCO^{3-}$, and $SO_4^{2-}$), and isotope (δD and δ18O) contents. This data aids in estimating reservoir temperatures using geothermometer equations. Surface characteristics of the South Zone manifestation reveal neutral to alkaline pH values (6.02 to 8.68), relative temperatures (29.97 to 42.57 °C), conductivity (49.8 to 100.7 mV), and TDS (Total Dissolved Solids) ranging from 352.6 to 497.0 mg/L. The dominant water composition is sodium–calcium–bicarbonate (Ca–Na–HCO3), indicating a bicarbonate water type. Average temperature depths in the South Zone manifestation of Mount Seulawah Agam are estimated as follows: Alue Ie Seu'um around 288.84 ± 2.19 °C, Alue Ie Masam around 304.17 ± 20.9 °C, Alue PU around 290.02 ± 6.85°C, and Alue Teungku around 265±11.39 °C. Isotope data (δD and δ18O) suggest meteoric water as the source for this manifestation. Fluid geochemical analysis indicates the potential for utilizing the geothermal manifestations of the South Zone of Mount Seulawah Agam for geothermal development or the construction of a geothermal power plant, given its high enthalpy system with an average temperature exceeding 225 °C. Further research, including data drilling, is essential to gather precise subsurface data. Additionally, the Aceh Provincial Government should formulate policies to identify strategic areas for geothermal development, leveraging the existing exploitable potential.

## 1. Introduction

Geothermal energy is a natural resource consisting of fluids (water and steam) stored in reservoirs and heated by rocks formed from magma solidifying at high temperatures [1–3]. Additionally, geothermal fluids ascend to the Earth's surface through fissures in rocks and are shown by various phenomena such as hot springs, mud pools, fumaroles, solfatara, and changes in rock formations [4]. Presently, the use of geothermal energy is highly diverse, encompassing electricity generation and non-electric applications like space heating, drying agricultural and livestock products, greenhouses, warm water pools, geothermal spas, and medicinal properties [5–7].

Geothermal energy in Seulawah Agam Mountain, Aceh Province-Indonesia, holds significant promise as a power source for plants with capacities of up to 55 MW [8]. With an estimated 29 GWe expected to originate from more than 300 sites, Indonesia has the greatest geothermal potential in the world [9, 10]. Based on geological and geochemical studies conducted by the Geological Agency in 2007, the geothermal system in Seulawah Agam was identified as part of the Great Sumatran fault system. The observed manifestation appears in the form of hot springs, presumed to be water reservoirs, which reach the ground surface without significant mixing with other water types [11]. Its characteristics include high water temperatures (around ±89 °C), clear water, neutral pH, and emergence in dacitic tufa rock units resulting from Seulawah Agam volcano activity, associated with silica deposits, and altered rocks [12].

In this study, an analysis was be conducted on the geochemical composition of geothermal water, encompassing the concentrations of cations ($K^+$, $Na^+$, $Ca^{2+}$, and $Mg^{2+}$) and anions ($Cl^-$, $HCO_3^-$, $SO_4^{2-}$) at the South Zone manifestation site of Mount Seulawah Agam, Aceh Besar Regency, Indonesia. The cations and anions under analysis are specific chemical elements used for geothermometer measurements and characterization of geothermal manifestation fluids. The resulting water geochemical data will be used to estimate the reservoir temperature of the geothermal system using the geothermometer equation [13]. Furthermore, based on the geochemical data, the type of geothermal fluid in the manifestation area will be figured out based on the relative concentrations of chloride ($Cl^-$), bicarbonate ($HCO_3^-$), and sulfate (SO42-) ions depicted in the ternary triangle diagram $Cl–HCO_3–SO_4$. This research will also investigate the characteristics of the fluids present in the manifestation area. By analyzing the geochemical data obtained from manifestations in the outflow area of Mount Seulawah Agam, we can learn the potential of the area as a source of geothermal energy.

The purpose of this research is to determine the predominant fluid type, geothermal fluid characteristics, and the source of geothermal water in Mount Seulawah Agam's South Zone. The objectives of this research are to provide information on dominant fluid types, define geothermal fluid characteristics, confirm the origin of source water, and determine the geothermal type (high or low enthalpy) in the area. Furthermore, it is expected that this study will serve as a reference for governmental bodies and higher education institutions to conduct additional research on the geothermal system on Mount Seulawah Agam and other volcanoes with the potential to use geothermal energy.

## 2. Materials and Methods

This research took place from November to December 2017. Characteristic analysis was conducted directly at the sampling site (in situ), while the analysis of geothermal fluid content was performed at the National Nuclear Energy Agency (BATAN) Laboratory in Pasar Jum'at, South Jakarta, Indonesia.

### *2.1. Tools and Materials*

The equipment utilized in this research includes a digital pH meter (Hanna Instruments), portable thermometer, digital TDS meter, digital conductometer (Milwaukee MW306 MAX Waterproof), GPS device (GARMIN), Ion Chromatography (IC) Instrument, Inductively Coupled Plasma–Optical Emission Spectrometry (ICP-OES) Instrument, Liquid Water Isotope Analyzer Instrument (LWIA), cool box, polyethylene bottles with capacities of 100 mL and 1000 mL, glass or plastic funnel, Whatman filter paper, universal pH indicator, stir bar, rubber gloves, dropper pipette, plastic bucket, and copper wire. The materials used include aqua bides water and diluted $HNO_3$.

### *2.2. Location and Sampling Method*

Geochemical water samples were collected from the manifestation area in the South Zone of Mount Seulawah Agam, which includes hot springs in the Alue Ie-Suum, Alue PU, Alue Ie Masam, and Alue Teungku areas in Seulimum District, Aceh Besar Regency, Aceh Province (Figure 1).

### *2.3. Water Sampling*

Water samples were collected from both hot springs and cold springs for comparison purposes. Samples of hot water were obtained from locations with the highest temperature and water discharge to minimize the risk of

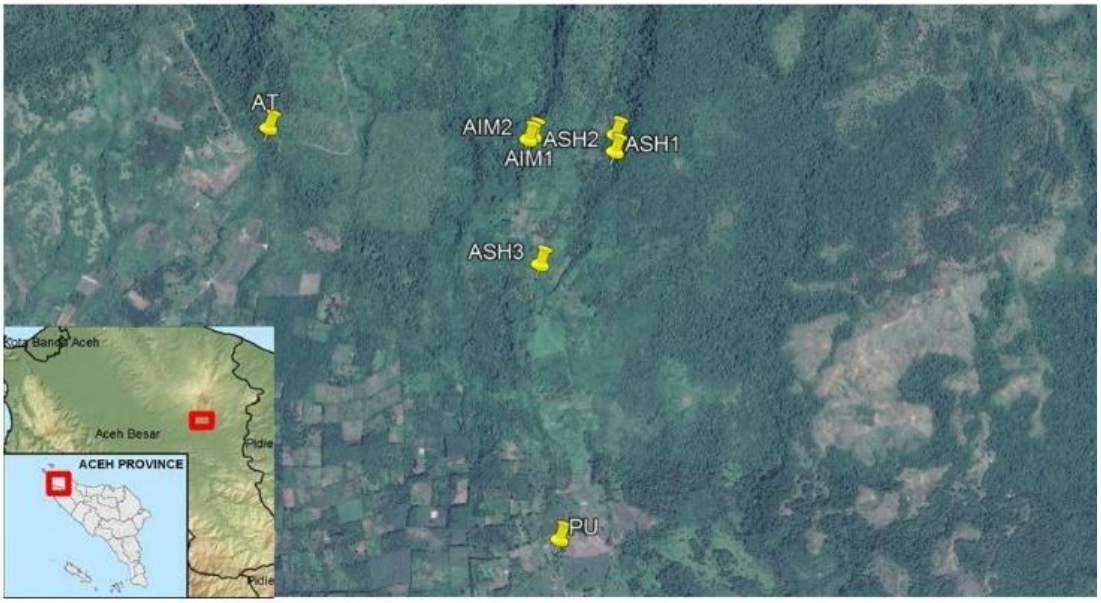


**Figure 1.** Google Earth satellite image of sampling points. Descriptions: Alue Ie-Suum (ASH 1-3), Alue PU (PU), Alue Ie Masam (AIM), and Alue Teungku (AT).

environmental contamination. The water samples were collected for two main purposes: elemental analysis and isotope analysis ($^{18}O$ and $^{2}H$). The equipment used for sampling and preparation included 500 mL capacity polyethylene bottles resistant to acid, heat, and corrosion, $^{18}O$ and $^{2}H$ isotope bottles with a capacity of 15 mL, made of glass covered with aluminum foil, Heat-resistant plastic syringe with a minimum capacity of 50 mL, Filter holder with a diameter of 25 mm, Filter paper with a porosity of 0.45 µm, GPS device, Altimeter, Stopwatch, Digital pH meter, pH paper, Conductivity meter, Heat-resistant rubber gloves, Camera, Work map and $HNO_3$ (Nitric Acid). The temperature of the manifestation and the surrounding air is measured using a thermocouple or thermometer, while a digital pH meter is utilized for measuring the pH of the water. The discharge of hot/cold water is measured using the volumetric method (V-notch meter), and the electrical conductivity of hot/cold water is determined using a conductometer. The coordinates and altitude of the sampling location were recorded using GPS.

Prior to sampling, the water to be collected must be filtered using filter paper with a porosity of 0.45 µm. The sampling bottle is cleaned using filtered water samples. The water sample is then divided into two bottles, each with a minimum volume of 500 mL. The first bottle is immediately labeled and designated for anion analysis (Cl, $HCO_3$, $SO_4$), while the second bottle is set aside before labeling and then acidified by adding $HNO_3$ in a 1:1 ratio until it reaches pH 2. This second bottle serves as the water sample for cation analysis (Na, K, Ca, Mg). Water samples collected from geothermal manifestations are initially filtered using Whatman filter paper and then divided into two separate parts, each stored in a different bottle. The first bottle is labeled as "acidified," indicating that the filtrate has been treated with a diluted $HNO_3$ solution to achieve a pH value of approximately ±2 using universal pH litmus paper. This water sample is intended for cation content analysis. The second bottle is labeled as "non-acidified," signifying that the filtrate remains untreated. This water sample is designated for anion content analysis. For water samples used to determine isotopes, the sample bottle is labeled with an isotope marker, indicating that it has been directly obtained from the hot spring with no air bubbles present and the bottle tightly sealed. This water sample is intended for $\delta^{18}O$ and $\delta D$ isotope analysis.

### *2.4. Inductively Coupled Plasma–Optical Emission Spectrometry (ICP–OES) Analysis Method*

Generally, the ICP-OES technique is utilized for ion analysis. The analysis stage of the ICP-OES technique includes sample preparation, target ion analysis, instrument calibration, and wavelength selection. A series of standard solutions is prepared for each cation to be tested. A minimum of four series of standard solutions are created with different concentrations to establish a linear equation. The water sample to be tested is diluted with distilled water (if necessary) and filtered to remove particulates. For samples containing solids, digestion is conducted using an acid solution and heating in a microwave oven. Some solids that are difficult to dissolve are reacted with compounds such as lithium metaborate or suitable solvents. This process is conducted synchronously between the instrument and

the computer (software). The method employed adheres to the predetermined equipment conditions, and the wavelength is configured for each analysis element. Standard solutions are measured, and samples are prepared. The spectrum data is generated in printout form, and the concentration of each required element is calculated [14].

*2.5. Ion Chromatography (IC) Analysis Method*

The water sample was injected and transported by the carbonate-bicarbonate solvent through the ion exchange column (separation column). Anions are separated based on their relative affinity at low capacity and ion exchange strength. Anion separation also occurs through a pressurized micromembrane. The pressure applied on the anion separation converts it into a high-conductivity acid, while the carbonate-bicarbonate solvent transforms into a weak-conductivity acid. The anion separation in their acid form is measured based on conductivity. Anions are identified by their retention time and compared with standard retention times. The concentration of anions in the sample is calculated based on the resulting area. A series of standard solutions is prepared for each cation to be tested. A minimum of four series of standard solutions are created with different concentrations to establish a linear equation known as a calibration curve. The standard solution is then allowed to equilibrate at room temperature before the test is conducted. The water sample to be tested is initially filtered using filter paper with a pore size of 0.45µm employing a syringe filter. This filtering process aims to purify the sample from impurities or particulates. Subsequently, the water sample is transferred into a clean vial and left to adjust to room temperature. The vial is then placed in the autosampler, and the IC instrument is operated according to the established method. The resulting chromatogram data is printed, and the required element concentrations are calculated [15].

*2.6. Liquid Water Isotope Analyzer (LWIA) Analysis Method*

Isotope analysis is conducted to ascertain the isotopic composition of water samples. The δD and $\delta^{18}O$ isotope composition of the water sample is then depicted on a Cartesian graph of δD (‰) against $\delta^{18}O$ (‰). The graph is subsequently compared with the global meteoric water line equation [16]. To prepare for analysis, four vials are arranged: two bottles for calibration, one bottle for control standards, and one bottle for blank. Another vial is filled with test samples, along with one vial containing deionized water for rinsing the syringe. All vials are positioned in the autosampler. The instrument is operated following established methods for isotope measurements, and the data are processed using IAEA (International Atomic Energy Agency) spreadsheet software.

*2.7. Data Analysis*

Data processing in this study entails determining geothermometer values for Na–K–Ca, Na–K–Mg, Na–K, and K–Mg. Additionally, geo-indicators are determined by constructing triangular ternary diagrams $Cl–SO_4–HCO_3$, Na/1000–K/100–K/Mg, and isotope graphs utilizing the liquid chemistry plotting spreadsheet version 3 method developed by Powell Geoscience Ltd. on September 3, 2012 by Powell & Cumming.

## 3. Results and Discussion

3.1. *Location and Characteristics of Surface Manifestations*

In-situ sampling and measurement of the characteristics of geothermal manifestations were conducted during the rainy season on November 19, 2017, at the geothermal manifestation points in the South Zone of Mount Seulawah Agam, including the Alue Ie Seu'um (ASH1, ASH2, and ASH3), Alue Ie Masam (AIM 1 and AIM 2), Alue PU, and Alue Teungku (AT) areas. Surface characteristic measurements comprise pH, conductivity (mV), Total Dissolved Solid (TDS) (mg/L), and surface temperature (°C). Manifestation characteristic measurements were performed in situ with five repetitions, each lasting 60 seconds per measurement, to ensure the accuracy of the field data. Additionally, the air temperature surrounding the manifestations was measured, and the coordinates and elevation were determined. The geothermal water sampling method is carried out proportionally, based on specific criteria and objectives, such as manifestation points with the highest surface temperatures and large discharges. The results of in-situ measurements of manifestation characteristics in the Alue Ie Seu'um, Alue Ie Masam, Alue PU, and Alue Teungku areas are shown in Table 1.

*3.1.1. Alue Ie Seu'um Manifestation Sampling Point*

The manifestation at Alue Ie Seu'um has three sampling points: ASH1, ASH2, and ASH3. At the ASH1 sampling point, the water was clear with a neutral pH (6.02±0.01), and there were gas bubbles around the manifestation. In the surrounding area, there are yellowish-brown iron oxide deposits and scorched bushes with a relatively large water discharge. ASH2 also has clear water without any gas bubbles, with a neutral pH (6.11±0.01), and around it, there are sintered travertine stones. The water discharge at ASH2 is the largest among the three sampling points. At ASH3, the water is also clear and

**Table 1.** Location and characteristics of geothermal surface manifestations in the South Zone of Mount Seulawah Agam.

| No. | Sampling Point | Coordinate | | Elevation (m) | $T_{air}$ (°C) | $T_{water}$ (°C) | pH | Conductivity (mV) | TDS (mg/L) |
|---|---|---|---|---|---|---|---|---|---|
| | | U | T | | | | | | |
| 1 | ASH 1 | 5°24'09" | 95°39'55" | 346 | 26.13 | 42.30 ± 0.05 | 6.02 ± 0.01 | 53.4 ± 0.43 | 425.2 ± 1.30 |
| 2 | ASH 2 | 5°24'05" | 95°39'54" | 347 | 26.19 | 42.57 ± 0.01 | 6.11 ± 0.01 | 55.7 ± 0.23 | 463.8 ± 2.59 |
| 3 | ASH 3 | 5°23'74" | 95°39'34" | 278 | 25.3 | 33.93 ± 0.01 | 7.28 ± 0.02 | 49.8 ± 0.47 | 352.6 ± 0.55 |
| 4 | AIM 1 | 5°24'09" | 95°39'32" | 359 | 24.8 | 35.66 ± 0.04 | 6.05 ± 0.01 | 55.1 ± 0.18 | 378.8 ± 3.27 |
| 5 | AIM 2 | 5°24'08" | 95°39'31" | 358 | 24.6 | 40.61 ± 0.08 | 6.07 ± 0.01 | 57.7 ± 0.20 | 497.0 ± 2.74 |
| 6 | PU | 5°24'11" | 95°38'61" | 164 | 24.7 | 30.01 ± 0.01 | 8.34 ± 0.01 | 71.3 ± 0.16 | 349.6 ± 0.89 |
| 7 | AT | 5°23'00" | 95°39'39" | 312 | 24.34 | 29.97 ± 0.01 | 8.68 ± 0.01 | 100.7 ± 0.31 | 372.8 ± 0.84 |

odorless, with a neutral pH (7.28±0.02), and there are small plants around it. The water discharge at ASH3 is also quite significant compared to ASH1. According to Table 1, the coordinates of the sampling points are 5°24'09'' N and 95°39'55" E, 5°24'05" N and 95°39'55" E and 5°23'74" N and 95°39'34" E (sequentially), with elevations of 346 meters above sea level, 347 meters above sea level, and 278 meters above sea level, respectively. Among the three manifestation points, ASH1 and ASH2 have the highest temperatures (42.30±0.05 °C and 42.57±0.01 °C) with a neutral pH. These two points also have higher conductivity and TDS (55.7±0.23 mV and 463.8±2.59 mg/L) compared to ASH3.

*3.1.2. Alue Ie Masam Sampling Point*

Water samples were collected from two points in the Alue Ie Masam manifestation, namely points AIM1 and AIM2. AIM1 features clear, odorless water with a neutral pH (6.02±0.01). Yellowish-brown iron oxide deposits are observed in the surrounding area, and the water flow is minimal. AIM2 exhibits similar characteristics to AIM1, with clear, odorless water and a neutral pH (6.02±0.01). However, the water discharge at AIM2 is greater than at AIM1. The coordinates of the Alue Ie Masam AIM1 sampling point are 5°24'09" N and 95°39'32" E, with an altitude of 359 meters above sea level, while AIM2 is located at coordinates 5°24'08" N and 95°39'31" E, with an elevation of 358 meters above sea level. AIM1 has lower temperature, conductivity, and TDS values compared to AIM2, with readings of 35.66±0.04 °C, 55.1±0.18 mV, and 378.8±3.27 mg/L, respectively. On the other hand, AIM2 exhibits higher temperature, conductivity, and TDS values compared to AIM1, with respective readings of 40.61±0.08 °C, 57.7±0.20 mV, and 497.0±2.74 mg/L.

*3.1.3. Alue Teungku Manifestation Sampling Point*

Sampling at the Alue Teungku (AT) manifestation was conducted at a single sampling point. The water at this point is clear, odorless, and has a neutral pH (8.34±0.01). Rocks and small plants surround the manifestation. The coordinates of this sampling point are 5°24'11" N and 95°38'61" E, with an elevation of 164 meters above sea level. Moreover, this sampling point exhibits low temperature but high conductivity and TDS, measuring 30.01±0.01 °C, 71.3±0.16 mV, and 349.6±0.89 mg/L, respectively.

*3.1.4. Alue PU Manifestation Sampling Point*

Sampling for the Alue PU manifestation was also conducted at a single point. The water in this manifestation is clear, odorless, and has a neutral pH (8.68±0.01). Surrounding the manifestation are rocks and small plants. This sampling point is located at coordinates 5°23'00" N and 95°39'39" E, with an elevation of 312 meters. Additionally, this sampling point has the lowest temperature but the highest conductivity and TDS, measuring 29.97 ± 0.01 °C, 100.7±0.31 mV, and 372.8±0.84 mg/L, respectively.

*3.2. Cation, Anion, and Isotope Analysis Results*

*3.2.1. Measurement Uncertainty*

All data analysis was performed using Powell Geoscience Ltd.'s Spreadsheet Version 3 (released on September 3, 2012), developed by Powell and Cumming. The uncertainty of the concentration measurements for each parameter is presented as standard deviation values. Additionally, various statistical function data were obtained using the LINEST method in Microsoft Excel. The calculation results yielded statistical function data, including the slope (m), standard deviation of the slope (Sm), intercept (b), standard deviation of the intercept (Sb), determination coefficient (R), standard deviation of the regression (Sr), and standard deviation of the concentration (SC) [11, 17].

*3.2.2. Analysis of Cation Content*

This study analyzed the concentrations of K, Na, Ca, and Mg cations. Cation concentration measurements were performed using ICP-OES, while reservoir temperature estimates were calculated using the geothermometer method. Calibration data from calculations of cation concentrations from geochemical water samples can be found in Table 2.

**Table 2.** Cation calibration using the ICP-OES method.

| Cations | Concentration Range (mg/L) | λ (nm) | Linearity | Coefficient of Determination ($R^2$) | Standard Regression ($Sr$) |
|---|---|---|---|---|---|
| $K^+$ | 1-20 | 766.490 | y = 507.3x + 358.7 | 0.9999999930 | 0.3622 |
| $Na^+$ | 1-20 | 818.326 | y = 60.31x - 248.4 | 0.9999990000 | 0.3824 |
| $Ca^{2+}$ | 1-20 | 184.006 | y = 91.98x - 0.741 | 0.9999960000 | 1.499 |
| $Mg^{2+}$ | 1-20 | 279.079 | y = 215.6x - 35.41 | 0.9998200000 | 24.891 |

**Table 3.** Cation concentrations in the South Zone manifestations of Mount Seulawah Agam using the ICP-OES Method.

| No. | Sampling Point | Na ± Sc (mg/L) | Mg ± Sc (mg/L) | Ca ± Sc (mg/L) | K ± Sc (mg/L) |
|---|---|---|---|---|---|
| 1 | ASH 1 | 58.11 ± 0.007 | 10.84 ± 0.127 | 91.74 ± 0.018 | 12.30 ± 0.002 |
| 2 | ASH 2 | 60.83 ± 0.006 | 47.57 ± 0.125 | 97.39 ± 0.017 | 12.45 ± 0.001 |
| 3 | ASH 3 | 50.99 ± 0.007 | 33.94 ± 0.126 | 75.31 ± 0.018 | 10.67 ± 0.002 |
| 4 | AIM 1 | 44.13 ± 0.008 | 32.20 ± 0.125 | 78.96 ± 0.018 | 9.24 ± 0.002 |
| 5 | AIM 2 | 77.52 ± 0.007 | 62.18 ± 0.125 | 113.84 ± 0.016 | 20.5 ± 0.001 |
| 6 | PU | 49.75 ± 0.007 | 34.47 ± 0.125 | 53.17 ± 0.017 | 10.47 ± 0.001 |
| 7 | AT | 49.75 ± 0.007 | 34.47 ± 0125 | 53.17 ± 0.017 | 10.47 ± 0.001 |

**Table 4.** Anion calibration using the IC method.

| Anion | Concentration Range (mg/L) | Linearity | Coefficient of Determination ($R^2$) | Standard Regression ($Sr$) |
|---|---|---|---|---|
| $Cl^-$ | 1-30 | y = 0.3369x - 0.0081 | 0.9995 | 0.09295 |
| $SO_4^{2-}$ | 1-30 | y = 0.1333x + 0.0031 | 0.9993 | 0.04429 |

**Table 5.** Anion concentration in the Manifestation of the South Zone of Mount Seulawah Agam using the IC method.

| No. | Sampling Point | $SO_4^{2-}$ ± Sc (mg/L) | $HCO_3^-$ (mg/L) | $Cl^-$ ± Sc (mg/L) |
|---|---|---|---|---|
| 1 | ASH 1 | 41.13 ± 0.412 | 566.7 | 11.16 ± 0.297 |
| 2 | ASH 2 | 34.25 ± 0.400 | 573.3 | 11.47 ± 0.298 |
| 3 | ASH 3 | 28.19 ± 0.389 | 454.4 | 13.62 ± 0.299 |
| 4 | AIM 1 | 28.19 ± 0.389 | 452.99 | 9.84 ± 0.296 |
| 5 | AIM 2 | 32.33 ± 0.386 | 602.05 | 20.76 ± 0.303 |
| 6 | PU | 30.57 ± 0.393 | 401.58 | 11.57 ± 0.298 |
| 7 | AT | 78.12 ± 0.470 | 384.67 | 13.06 ± 0.299 |

The results of testing cation concentrations in the manifestation areas of Alue Ie Seu'um (ASH1, ASH2, and ASH3), Alue Ie Masam (AIM1 and AIM2), Alue PU, and Alue Teungku (AT) are provided in Table 3. Calculation of cation concentrations in this study was carried out based on linearity (equation of lines). The cation concentrations obtained were used to estimate the reservoir temperature and its characteristics using the geothermometer equation, as well as to characterize surface water in geothermal manifestations in the South Zone of Mount Seulawah Agam.

*3.2.3. Analysis of Anion Content*

The anions measured in this study include Cl and $SO_4$. Anion concentration measurements were carried out using Ion Chromatography (IC), while for measuring bicarbonate ions ($HCO_3$), the acidimetric (acid-base) titration method was used [11, 18]. Information regarding calibration data from calculations of anion concentrations from geochemical water samples can be seen in Table 4.

The results of anion concentration testing in the manifestation areas of Alue Ie Seu'um (ASH1, ASH2, and ASH3), Alue Ie Masam (AIM1 and AIM2), Alue PU, and Alue Teungku (AT) in the South Zone of Mount Seulawah Agam can be seen in Table 5. The calculation of anion concentration in this study is based on linearity (equation of lines). The anion concentrations obtained are used to elucidate the characteristics of geothermal fluid types in each manifestation in the South Zone of Mount Seulawah Agam.

*3.2.4. Isotope Analysis*

The isotopes measured in this study were oxygen ($\delta^{18}O$) and deuterium ($\delta^{2}H$), whose measurements were carried out using the Liquid Water Isotope Analyzer (LWIA) instrumentation. The results of testing isotope values in the manifestation areas of Alue Ie Seu'um (ASH1, ASH2,

**Table 6.** Oxygen ($\delta^{18}O$) and Deuterium ($\delta^{2}D$) isotope values in the manifestation area of the South Zone of Mount Seulawah Agam.

| No. | Sampling Point | $\delta O^{18}$ (‰) | $\delta D$ (‰) |
|---|---|---|---|
| 1 | ASH 1 | -10.36 ± 0.20 | -55.9 ± 0.6 |
| 2 | ASH 2 | -8.99 ± 0.67 | -54.7 ± 0.9 |
| 3 | ASH 3 | -9.37 ± 0.19 | -57.4 ± 0.5 |
| 4 | AIM 1 | -9.82 ± 0.19 | -55.2 ± 0.7 |
| 5 | AIM 2 | -9.78 ± 0.22 | -57.1 ± 0.9 |
| 6 | PU | -10.00 ± 0.26 | -53.8 ± 0.9 |
| 7 | AT | -9.56 ± 0.61 | -61.4 ± 0.8 |

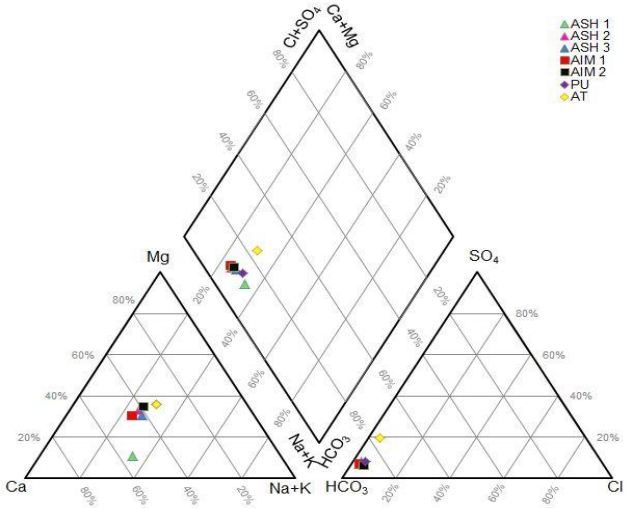


**Figure 2.** The Piper diagram for the manifestation area in the South Zone of Mount Seulawah Agam [19].

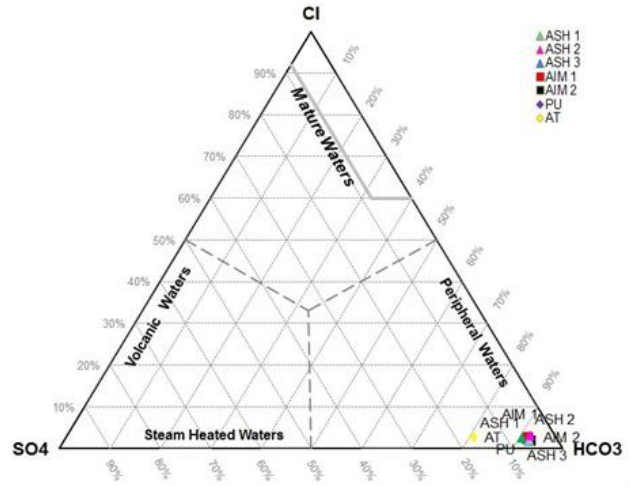


**Figure 3.** The Cl-$HCO_3$-$SO_4$ Triangle Diagram for the manifestation area in the South Zone of Mount Seulawah Agam [20].

and ASH3), Alue Ie Masam (AIM1 and AIM2), Alue PU, and Alue Teungku (AT) in the South Zone of Mount Seulawah Agam can be seen in Table 6. The calculation of isotope values in this study is linked to the international standard line V-SMOW, which is used to elucidate hot springs or the origin of water (Meteoric/ Magmatic water) in each manifestation in the South Zone of Mount Seulawah Agam.

### *3.3. Chemical Composition and Water Type*

The characteristics of geothermal water can be determined based on the composition of geochemical elements, often depicted in a Piper diagram. Figure 2 illustrates the South Zone area of Mount Seulawah Agam, encompassing the manifestations of Alue Ie Seu'um (ASH1, ASH2, and ASH3), Alue Ie Masam (AIM1 and AIM2), Alue PU, and Alue Teungku (AT). The plot diagram results indicate three types of fluid: cation-chloride, cation-bicarbonate water, and cation-sulfate [19].

Based on the analysis of cations and anions in the manifestations of Alue Ie Seu'um (ASH1, ASH2, and ASH3), Alue Ie Masam (AIM1 and AIM2), Alue PU, and Alue Teungku (AT), it can be concluded that these manifestations are dominated by sodium-calcium-bicarbonate (Ca-Na-$HCO_3$) cations. This manifestation is often referred to as neutral bicarbonate water with high temperatures and a pH close to neutral, which is formed due to the reaction of geothermal fluids with local rocks [21].

The type of geothermal fluid can be determined based on the dominant anion. Each manifestation has a different fluid type. Determining the type of geothermal fluid in the manifestations of Alue Ie Seu'um (ASH1, ASH2, and ASH3), Alue Ie Masam (AIM1 and AIM2), Alue PU, and Alue Teungku (AT) is carried out using a Cl-$HCO_3$-$SO_4$ triangle diagram plot. Based on the results of anion analysis, all these manifestations indicate a bicarbonate fluid type. This indicates that the geothermal fluid in the South Zone of Mount Seulawah Agam originates from a shallow reservoir mixed with rocks or other fluids [22]. This manifestation is also known as neutral bicarbonate and is often found in outflow areas with shallow reservoir depths, high temperatures, and near-neutral pH produced by the interaction of fluids with rocks when they reach the surface [21].

The classification of geothermal water types is based on the predominant anion concentrations, as represented by the Cl-$HCO_3$-$SO_4$ ternary diagram (Figure 3). This diagram illustrates that the water at all points of manifestation is of the bicarbonate type.

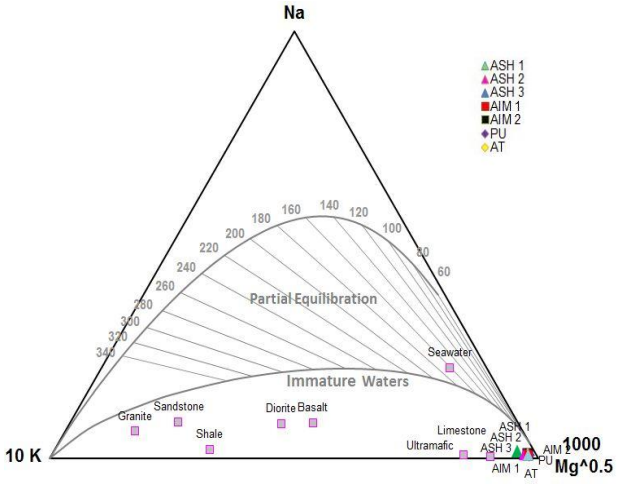


**Figure 4.** The Na-K-Mg Triangle Diagram for the manifestation area in the South Zone of Mount Seulawah Agam [20].

### *3.4. Na–K–Mg Triangle Diagram in Manifestation*

The Na-K-Mg geothermometer method is highly valuable for assessing reservoir conditions and conditions near the surface. This method combines two distinct geothermometer equations, namely Na-K and K-Mg. The Na-K equation reflects the slow reaction equilibrium process in the reservoir, while the K-Mg equation reflects the fast reaction equilibrium process in areas closer to the surface. To utilize a Na-K-Mg geothermometer, chemical data of sodium (Na), potassium (K), and magnesium (Mg) for each hot spring are required, and then the data will be plotted on a triangular diagram.

From Figure 4, it can be inferred that the manifestations in the South Zone of Mount Seulawah Agam, including Alue Ie Seu'um (ASH1, ASH2, and ASH3), Alue Ie Masam (AIM1 and AIM2), Alue PU, and Alue Teungku (AT), exhibit characteristics of Immature Waters (partial equilibrium). This indicates an immature water condition, as there is no equilibrium dissolution of Na-K and K-Mg minerals in deep reservoirs, and it is influenced by the dissolution of other minerals upon reaching the surface. This condition suggests a mixture of surface water and fluid during the formation of hot springs. Additionally, hot water is influenced by the interaction between hot water and rocks [20].

### *3.5. Geothermal Manifestation Geothermometers*

Geothermometers are a method utilized to estimate subsurface (reservoir) temperatures based on the chemical dependency (solution or gas) on temperature principle. This method is frequently employed in evaluating the geothermal potential of a region and in other scientific inquiries. A compilation of equilibrium chemical equations that are temperature-dependent is referred to as a geothermometer. For instance, the solubility of salt increases with rising temperature. Therefore, by knowing the composition of the salt, the equilibrium temperature at which the salt will dissolve can be approximated. However, the processes occurring within the earth are significantly more intricate than those taking place in a laboratory setting. Consequently, in interpreting geothermometer data, assumptions and consistency among various geothermometer calculations are required. The results of different geothermometer calculations for geothermal manifestations in the South Zone of Mount Seulawah Agam are presented in Table 7.

#### *3.5.1. Na-K-Ca Geothermometer*

The Na-K-Ca geothermometer is an equation utilized to estimate reservoir temperatures in geothermal systems with relatively high Ca concentrations in fluids. This equation provides accurate results within temperature ranges of 120-200 °C [23]. Based on the Na-K-Ca geothermometer results in Table 7, it can be inferred that all manifestation points in the South Zone of Mount Seulawah Agam have reservoir temperatures below 180 °C. This is attributed to the low Ca content in this region's manifestations, which ensures that the ratio of Na-K-Ca minerals from depth remains unaffected by the Ca content in equilibrium [16].

#### *3.5.2. K-Mg Geothermometer*

The K-Mg geothermometer was first applied to manifestations with shallow depth temperatures ranging from 120-140 °C [20]. However, this equation is not yet suitable for subsequent calculations compared to Na-K and Na-K-Ca geothermometers, as the geothermal fluid has not reached mineral equilibrium. According to the results of K-Mg geothermometer calculations in Table 7, it can be deduced that manifestations in Alue Ie Seu'um (ASH1, ASH2, and ASH3), Alue Ie Masam (AIM1 and AIM2), Alue PU, and Alue Tengku (AT) have reservoir temperatures less than 120 °C. This is due to the mixing of geothermal fluid and surface water (Mg > 1 mg/L), which affects the depth temperature calculation [16]. Therefore, based on these findings, this geothermometer is not suitable for use in the South Zone of Mount Seulawah Agam, Aceh Besar.

#### *3.5.3. Na-K Geothermometer*

The Na-K geothermometer is a method used to estimate reservoir temperatures in high-temperature reservoirs and has been developed by several researchers based on systematic variations in Na and K content [23]. This geothermometer is suitable for geothermal fluids with reservoir temperatures ranging from 180-350 °C and low calcium content (CCa½/CNa<1), but it is not suitable for temperatures below 120 °C. Based on the results

**Table 7.** Data from manual geothermometer calculations for the manifestation area in the South Zone of Mount Seulawah Agam.

| No. | Sampling Point | Na-K-Ca (Fournier & Truesdell (°C) | Na/K Fournier (°C) | Na/K Truesdell (°C) | Na/K Giggenbach (°C) | Na/K Tonani (°C) | Na/K Nieva & Nieva (°C) | Na/K Arnorsson (°C) | K/Mg Giggenbach (°C) |
|---|---|---|---|---|---|---|---|---|---|
| 1 | ASH 1 | 66.8 | 291.0 | 285.5 | 300.2 | 334.0 | 276.2 | 286.4 | 69.9 |
| 2 | ASH 2 | 66.4 | 287.2 | 280.2 | 296.8 | 328.0 | 272.5 | 281.6 | 53.8 |
| 3 | ASH 3 | 65.2 | 289.7 | 283.7 | 299.0 | 331.9 | 274.9 | 284.8 | 54.1 |
| 4 | AIM 1 | 58.5 | 289.7 | 283.8 | 299.1 | 332.0 | 275.0 | 284.8 | 51.7 |
| 5 | AIM 2 | 81.1 | 315.9 | 320.9 | 322.7 | 374.7 | 300.6 | 318.9 | 61.4 |
| 6 | PU | 71.4 | 290.3 | 284.6 | 299.6 | 333.0 | 275.6 | 285.6 | 53.6 |
| 7 | AT | 56.6 | 268.6 | 254.7 | 279.9 | 298.9 | 254.3 | 258.0 | 49.1 |

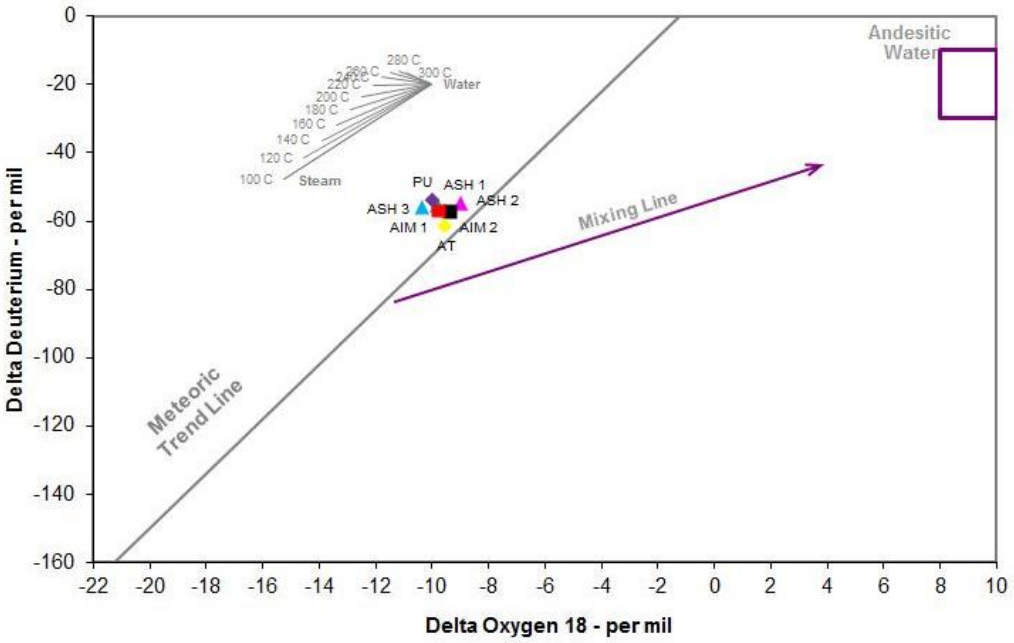


**Figure 5**. The isotopic ratios graph in the South Zone manifestation area of Mount Seulawah Agam.

presented in Table 7, the estimated reservoir temperatures for the Alue Ie Seu'um manifestations (ASH1, ASH2, and ASH3) using the Na-K geothermometer averaged 290.77±6.72 °C, 286.45±7.53 °C, and 289.3±6.97 °C (respectively). For the Alue Ie Masam manifestation (AIM1 and AIM2), the estimated reservoir temperatures averaged 289.35±6.99 °C and 319±2.91 °C (respectively). Meanwhile, for the Alue PU and Alue Tengku (AT) manifestations, the estimated reservoir temperatures averaged 290.02±6.85 °C and 265±11.39 °C (respectively). This geothermometer equation can be relied upon to estimate reservoir temperatures in the South Zone manifestations of Mount Seulawah Agam, Aceh Besar, as the results are within the applicable range of the Na-K geothermometer [17, 23, 24].

*3.6. Isotopes*

This study primarily focuses on analyzing the content of stable isotopes. Common stable isotopes used in geothermal research include hydrogen (1H, 2H, or deuterium, D) and oxygen ($^{16}O$, $^{18}O$). These isotopes offer insights into the processes and origins of water. The δD content in geothermal fluids is comparable to that of meteoric water, while the $\delta^{18}O$ value in geothermal fluids tends to be more positive than meteoric water [16]. Changes in $\delta^{18}O$ values can occur due to exchanges with heavier isotopes. Some isotope data indicate that the contribution of magmatic fluid to geothermal fluid is generally small (around 5-10% of the total fluid), with the majority originating from meteoric water. The influence of magmatic fluid is typically reflected in the difference in δD values between geothermal fluid and meteoric water [16]. The stable isotopes analyzed in the warm water samples in this research area are D and $^{18}O$. These two isotopic values aid in determining whether the hot fluid in the geothermal system in the study area originates from meteoric water or magmatic fluid. Based on the data of deuterium and oxygen-18 isotope values (Table 6), the third hot spring is situated near the blue line, representing the Global Meteoric Water Line (GMWL)

(Figure 5). This indicates that the water source for the geothermal system in the South Zone of Mount Seulawah Agam originates from meteoric precipitation.

This research has several limitations in its implementation. For example, the limited number and representativeness of geochemical samples can affect the accuracy and generalizability of research results. In addition, difficult access to geological locations or dangerous environmental conditions can make sampling difficult and expensive. Geochemical processes are often complex because they involve interactions between various geological, hydrological, and biological factors [11, 25]. Understanding these interactions requires deep understanding and is often difficult to fully study. Geochemical data is often related to hearths, especially when derived from complex analysis methods or difficult-to-reach locations. In addition, the interpretation of geochemical data can be subjective and highly dependent on the researcher's knowledge and experience.

Regarding the future, there are several potential developments that can be explored. One way is through the development of new analytical methods and increasing the sensitivity and accuracy of geochemical analysis [26, 27]. This can help deepen understanding of the geochemical processes that occur in various environmental contexts. In addition, the integration of geochemical data with data from other disciplines, such as geophysics, geology, and hydrology, can provide a more holistic picture of geological systems and the processes that occur. Case studies that are more detailed and involve various scientific disciplines can provide deeper insight into the complexity of geochemical systems at various locations [28]. The application of geochemical techniques for environmental monitoring can also make an important contribution to understanding patterns of environmental change, including pollution problems and climate change [29, 30]. Finally, the utilization of new technologies such as miniature geochemical sensors, sophisticated spectroscopic analysis, and the use of more advanced computer modeling can open new opportunities in the field of geochemical studies [31].

## 4. Conclusions

Based on the field research results and fluid geochemistry analysis of the geothermal manifestations in the South Zone of Mount Seulawah Agam, it can be concluded that the surface characteristics for the manifestations in the South Zone of Mount Seulawah Agam show neutral to slightly alkaline pH values, ranging from 6.02 to 8.68. The temperatures are relatively warm, ranging from 29.97 to 42.57 °C. The conductivity values range from 49.8 to 100.7 mV, while the Total Dissolved Solids (TDS) range from 352.6 to 497.0 mg/L. The dominant composition for cations and anions in the manifestations in the South Zone of Mount Seulawah Agam is sodium-calcium-bicarbonate (Na-Ca-$HCO_3$), indicating that the dominant type of water is bicarbonate water. The estimated depth temperatures using geothermometers in the manifestations in the South Zone of Mount Seulawah Agam show the following results: Alue Ie Seu'um has an average temperature of 288.84±2.19 °C. Alue Ie Masam has an average temperature of 304.17±20.9 °C. Alue PU has an average temperature of 290.02±6.85 °C. Alue Teungku has an average temperature of around 265±11.39 °C. The D and $^{18}O$ isotope data indicate that the water source in the South Zone of Mount Seulawah Agam originates from meteoric water. Fluid geochemistry analysis indicates that the geothermal manifestations in the South Zone of Mount Seulawah Agam have the potential to be developed as geothermal areas or power plant construction sites. These findings are based on analyses in the research area indicating the presence of a high-temperature geothermal system (high enthalpy) characterized by average temperatures of over 225 °C.

**Author Contributions:** Conceptualization, A.L. and R.I.; methodology, M.Y.; software, M.Y.; validation, A.L., M.Y., S.S and R.I.; formal analysis, R.I.; investigation, A.L.; resources, A.L.; data curation, R.I.; writing—original draft preparation, A.L. and R.S.; writing—review and editing, N.B.M.; visualization, A.L.; supervision, A.L.; project administration, N.B.M.; funding acquisition, D.D. All authors have read and agreed to the published version of the manuscript.

**Funding:** This study does not receive external funding.

**Ethical Clearance:** Not applicable.

**Informed Consent Statement:** Not applicable.

**Data Availability Statement:** Not applicable.

**Acknowledgments:** Not applicable.

**Conflicts of Interest:** All the authors declare that there are no conflicts of interest.

## References

1. Hochstein, M. P., and Sudarman, S. (2008). History of Geothermal Exploration in Indonesia from 1970 to 2000, *Geothermics*, Vol. 37, No. 3, 220–266. doi:10.1016/j.geothermics.2008.01.001.
2. Soltani, M., Moradi Kashkooli, F., Souri, M., Rafiei, B., Jabarifar, M., Gharali, K., and Nathwani, J. S. (2021). Environmental, Economic, and Social Impacts of Geothermal Energy Systems, *Renewable and Sustainable Energy Reviews*, Vol. 140, 110750. doi:10.1016/j.rser.2021.110750.
3. Lund, J. W., and Toth, A. N. (2021). Direct Utilization of Geothermal Energy 2020 Worldwide Review, *Geothermics*, Vol. 90, 101915. doi:10.1016/j.geothermics.2020.101915.

4. Xiong, Y., Zhu, M., Li, Y., Huang, K., Chen, Y., and Liao, J. (2022). Recognition of Geothermal Surface Manifestations: A Comparison of Machine Learning and Deep Learning, *Energies*, Vol. 15, No. 8. doi:10.3390/en15082913.
5. Aprianto, A., Maulana, A., Noviandy, T. R., Lala, A., Yusuf, M., Marwan, M., Afidh, R. P. F., Irvanizam, I., Nizamuddin, N., and Idroes, G. M. (2023). Exploring Geothermal Manifestations in Ie Jue , Indonesia : Enhancing Safety with Unmanned Aerial Vehicle, *Leuser Journal of Environmental Studies*, Vol. 1, No. 2, 47–54. doi:10.60084/ljes.v1i2.75.
6. Maulydia, N. B., Idroes, R., Khairan, K., Tallei, T. E., and Mohd Fauzi, F. (2024). Ecotoxicological Insight of Phytochemicals, Toxicological Informatics, and Heavy Metal Concentration in Tridax procumbens L. in Geothermal Areas, *Global Journal of Environmental Science and Management*, Vol. 10, No. 1, 369–384. doi:10.22034/gjesm.2024.01.23.
7. Maulydia, N. B., Khairan, K., Tallei, T. E., Estevam, E. C., Patwekar, M., Mohd Fauzi, F., and Idroes, R. (2023). GC-MS Analysis Reveals Unique Chemical Composition of Blumea balsamifera (L.) DC in Ie-Jue Geothermal Area, *Grimsa Journal of Science Engineering and Technology*, Vol. 1, No. 1, 9–16. doi:10.61975/gjset.v1i1.6.
8. Darma, S., Imani, Y. L., Naufal, M., Shidqi, A., Riyanto, D., and Yunus Daud, M. (2020). Country Update: The Fast Growth of Geothermal Energy Development in Indonesia, *Proceedings World Geothermal Congress 2020+1*, No. 12, 8.
9. Bertani, R. (2016). Geothermal Power Generation in the World 2010–2014 Update Report, *Geothermics*, Vol. 60, No. October 2021, 31–43. doi:10.1016/j.geothermics.2015.11.003.
10. Deon, F., Förster, H.-J., Brehme, M., Wiegand, B., Scheytt, T., Moeck, I., Jaya, M. S., and Putriatni, D. J. (2015). Geochemical/Hydrochemical Evaluation of the Geothermal Potential of the Lamongan Volcanic Field (Eastern Java, Indonesia), *Geothermal Energy*, Vol. 3, No. 1, 20. doi:10.1186/s40517-015-0040-6.
11. Idroes, R., Yusuf, M., Saiful, S., Alatas, M., Subhan, S., Lala, A., Muslem, M., Suhendra, R., Idroes, G. M., Marwan, M., and Mahlia, T. M. I. (2019). Geochemistry Exploration and Geothermometry Application in the North Zone of Seulawah Agam, Aceh Besar District, Indonesia, *Energies*, Vol. 12, No. 23, 4442. doi:10.3390/en12234442.
12. Marwan, Rusydy Ibnu , Nugraha Gartika Setiya, A. (2014). Study of Seulawah Agam's Geothermal Source Using Gravity Method, *Natural*, Vol. 14, No. 2, 1–5. doi:10.17969/jn.v14i2.2252.
13. Putri, D. R., N. Ismail, R. Idroes, M. Marwan, S. Rizal, Abdulmadjid, S. N., Idroes, G. M., Noviandy, T. R., A. Lala, M. Yusuf, M. Muslem, R. Suhendra, M. Yanis, and D. B. Dharma. (2023). Geochemical Investigation of Hot Springs in the Bur Ni Geureudong Geothermal Prospect Area, Aceh-Indonesia, *RASAYAN Journal of Chemistry*, Vol. 16, No. 03, 1826–1834. doi:10.31788/RJC.2023.1638430.
14. Wilschefski, S., and Baxter, M. (2019). Inductively Coupled Plasma Mass Spectrometry: Introduction to Analytical Aspects, *Clinical Biochemist Reviews*, Vol. 40, No. 3, 115–133. doi:10.33176/AACB-19-00024.
15. Rosydiati. (2019). Karakterisasi Puncak Kromatogram dalam High Performance Liquid Chromatography (HPLC) terhadap Perbedaan Fase Gerak, Laju Alir, dan Penambahan Asam dalam Analisis Indole Acetic Acid (IAA), *Kandaga*, Vol. 1, No. 2, 65–73.
16. Nicholson, K. (1993). Geothermal Fluids: Chemistry and Exploration Techniques, *Springer Verlag*, Vol. 263.
17. Idroes, R., Yusuf, M., Alatas, M., Subhan, Lala, A., Saiful, Suhendra, R., Idroes, G. M., and Marwan. (2018). Geochemistry of Hot Springs in the Ie Seu'um Hydrothermal Areas at Aceh Besar District, Indonesia, *IOP Conference Series: Materials Science and Engineering*, Vol. 334, No. 1, 012002. doi:10.1088/1757-899X/334/1/012002.
18. Idroes, R., Yusuf, M., Alatas, M., Subhan, Lala, A., Muslem, Suhendra, R., Idroes, G. M., Suhendrayatna, Marwan, and Riza, M. (2019). Geochemistry of Warm Springs in the Ie Brôuk Hydrothermal Areas at Aceh Besar District, *IOP Conference Series: Materials Science and Engineering*, Vol. 523, 012010. doi:10.1088/1757-899X/523/1/012010.
19. Piper, A. M. (1944). A Graphic Procedure in the Geochemical Interpretation of Water-Analyses, *Transactions, American Geophysical Union*, Vol. 25, No. 6, 914. doi:10.1029/TR025i006p00914.
20. Giggenbach, W. F. (1988). Geothermal Solute Equilibria. Derivation of Na-K-Mg-Ca Geoindicators, *Geochimica et Cosmochimica Acta*, Vol. 52, No. 12, 2749–2765. doi:10.1016/0016-7037(88)90143-3.
21. Mahon, W. A. J., Klyen, L. E., and Rhode, M. (1980). Neutral Sodium/Bicarbonate/Sulfate Hot Waters in Geothermal Systems.
22. Tsutsui, W. M. (1996). W. Edwards Deming and the Origins of Quality Control in Japan, *Journal of Japanese Studies*, Vol. 22, No. 2, 295. doi:10.2307/132975.
23. Fournier, R. O., and Truesdell, A. H. (1973). An Empirical Na K Ca Geothermometer for Natural Waters, *Geochimica et Cosmochimica Acta*, Vol. 37, No. 5, 1255–1275. doi:10.1016/0016-7037(73)90060-4.
24. Idroes, R., Yusuf, M., Alatas, M., Subhan, Lala, A., Muhammad, Suhendra, R., Idroes, G. M., and Marwan. (2019). Geochemistry of Sulphate Spring in the Ie Jue Geothermal Areas at Aceh Besar District, Indonesia, *IOP Conference Series: Materials Science and Engineering*, Vol. 523, No. 1, 012012. doi:10.1088/1757-899X/523/1/012012.
25. Stracke, A. (2021). A Process-Oriented Approach to Mantle Geochemistry, *Chemical Geology*, Vol. 579, 120350. doi:10.1016/j.chemgeo.2021.120350.
26. Balaram, V. (2021). Current and Emerging Analytical Techniques for Geochemical and Geochronological Studies, *Geological Journal*, Vol. 56, No. 5, 2300–2359. doi:10.1002/gj.4005.
27. Balaram, V. (2021). New Frontiers in Analytical Techniques — Opportunities and Challenges in Geochemical Research, *Journal of the Geological Society of India*, Vol. 97, No. 4, 331–334. doi:10.1007/s12594-021-1690-6.
28. Puetz, S. J., Condie, K. C., Sundell, K., Roberts, N. M. W., Spencer, C. J., Boulila, S., and Cheng, Q. (2024). The Replication Crisis and Its Relevance to Earth Science Studies: Case Studies and Recommendations, *Geoscience Frontiers*, Vol. 15, No. 4, 101821. doi:10.1016/j.gsf.2024.101821.
29. Xu, H., and Zhang, C. (2023). Development and Applications of GIS-Based Spatial Analysis in Environmental Geochemistry in the Big Data Era, *Environmental Geochemistry and Health*, Vol. 45, No. 4, 1079–1090. doi:10.1007/s10653-021-01183-8.
30. Lemière, B., and Uvarova, Y. A. (2020). New Developments in Field-Portable Geochemical Techniques and On-Site Technologies and Their Place in Mineral Exploration, *Geochemistry: Exploration, Environment, Analysis*, Vol. 20, No. 2, 205–216. doi:10.1144/geochem2019-044.
31. Chen, T., Zhang, T., and Li, H. (2020). Applications of Laser-Induced Breakdown Spectroscopy (LIBS) Combined with Machine Learning in Geochemical and Environmental Resources Exploration, *TrAC Trends in Analytical Chemistry*, Vol. 133, 116113. doi:10.1016/j.trac.2020.116113.